A Low Complexity Model Order and Frequency Estimation of Multiple 2-D Complex Sinusoids

Vesna Popović–Bugarin[a], Slobodan Djukanović[a,*]

[a] *University of Montenegro/Faculty of Electrical Engineering*
Džordža Vašingtona bb, 81 000, Podgorica, Montenegro
e-mail: {pvesna, slobdj}@ucg.ac.me
web: http://www.tfsa.ac.me

Abstract

Model order and frequency estimation of multiple 2-D complex sinusoids in additive white Gaussian noise are addressed. Frequency estimation follows the coarse-fine search strategy. Coarse estimates, obtained by locating maxima of the 2-D discrete Fourier transform, are refined in a two-stage procedure. In both stages, frequency refinement is based on three-point periodogram maximization. In order to provide accurate model order estimation (MOE) for a wide signal-to-noise ratio (SNR) range, our approach combines two metrics for sinusoid detection in the 2-D frequency domain, one for low and the other for high SNR values. The proposed frequency estimation attains the Cramér-Rao lower bound and it outperforms parametric methods in terms of the estimation accuracy and numerical efficiency. Compared with information criterion-based methods, the proposed MOE is numerically more efficient, it does not require estimation of noise variance and therefore does not suffer from overestimation at high SNR.

Keywords: Multidimensional signal processing, discrete Fourier transform, frequency estimation, Cramér-Rao bound, probability of false alarm

1. Introduction

Frequency estimation of multiple 2-D sinusoids represents an important issue in numerous areas, including sensor array processing, wireless communications, ultrasound imaging, sonar and radar [1–6]. In planar sensor arrays (PSAs), for example, frequency components of a 2-D sinusoid are related to the azimuth and elevation angles of the signal source, i.e., direction-of-arrival (DOA) in PSAs reduces to frequency estimation [7, 8]. Frequency estimation approaches can be broadly divided into two categories, non-parametric and parametric ones. The most widely used non-parametric approach is based on 2-D spectral estimation performed via computationally attractive 2-D discrete Fourier transform (DFT). For large datasets, this

*Corresponding author
Email address: slobdj@ucg.ac.me (Slobodan Djukanović)

approach yields satisfactory estimation accuracy. However, with smaller datasets, it suffers from the Fourier resolution limit.

Instead of analyzing the signal in the frequency domain, the parametric-based approaches usually treat it in the original time domain. Maximum likelihood (ML) method [9, 10], a representative of this class, is a computationally exhaustive approach. Subspace-based methods have been developed in order to alleviate the ML computational complexity and they separate the received signal into sinusoid and noise subspaces by means of eigenvalue decomposition or singular value decomposition. This class includes signal parameters via rotational invariance technique (ESPRIT) [4, 11], matrix enhancement and matrix pencil (MEMP) [1], modified MEMP (MMEMP) which resolves the frequency-pairing problem encountered in the MEMP method [3], principal-singular-vector utilization for modal analysis (PUMA) [5], multidimensional folding (MDF) [12] and improved MDF (IMDF) [2]. A significant disadvantage of the subspace-based frequency estimation methods is high computational complexity, which can be additionally increased by the frequency-pairing problem [1]. In addition, when two or more frequencies along one dimension coincide, some of these methods fail to separate 2-D components correctly, which, in turn, results in severe performance degradation [2].

In the aforementioned methods, the number of 2-D complex sinusoids (model order) is known in advance. In practice, however, this is often not the case. Model order estimation (MOE) in the presence of noise is an important and challenging issue [13–18]. It has been investigated thoroughly for 1-D signals and generally considered separately from the frequency estimation problem [15–17, 19]. The most popular MOE techniques, namely Bayesian Information Criteria (BIC), Akaike Information Criteria (AIC), adaptively penalized likelihood approach (PAL) and exponentiation embedded family (EEF) have been recently generalized for 2-D complex exponential signals [13]. In these techniques, identification of correct model order is carried out via minimizing a penalized-likelihood function calculated for a set of candidate model orders. To ensure that the true model order is within the set, its cardinality has to be set high, which represents a computational overhead. Moreover, for each candidate order, the ML frequency estimation of signal components is used [13, 15, 16], which is a computationally demanding approach [9, 10]. Another drawback of the information criterion-based MOE techniques is performance deterioration due to poor noise variance estimation. Namely, at high SNR, residuals of the extracted components affect the noise variance estimation resulting in overestimation of the number of components [6, 13, 15–17].

In [14], a subspace-based approach for detecting 2-D complex sinusoids corrupted by additive white Gaussian noise (AWGN) and their parameter estimation is proposed. It is a 2-D extension of the frequency counterpart of the ESPRIT method. Being 2-D spectrum area-selective, its computational complexity is reduced compared to standard time-domain subspace-based methods [1–5, 11, 12]. However, a restriction of [14] is that all frequencies are distinct in all dimensions.

An effective and accurate interpolation-based method (IBM) for frequency estimation of noisy 1-D com-

plex sinusoids is proposed in [20] and extended to 2-D sinusoids in [21]. In IBM, both the frequencies and amplitude of each component are estimated after the leakage terms of other components have been iteratively removed. In addition, it works with a known model order.

In this paper, we consider model order and frequency estimation of multiple 2-D complex sinusoids embedded in AWGN. Our non-parametric approach operates in the frequency domain. Maxima of the 2-D periodogram correspond to approximate location of sinusoids in the 2-D frequency plane. Coarse frequency estimation is, therefore, performed by locating periodogram maxima on the frequency grid. Since the true sinusoid frequencies generally do not coincide with the grid values, a refinement is needed to improve the estimation accuracy. Refinement is performed in two stages. In the first stage, MOE is carried out and coarse frequency estimations refined. The second stage represents an additional refinement step in which, prior to frequency estimation, the influence of components on the one currently estimated is suppressed. The proposed method outperforms parametric methods [2, 3, 11] in terms of estimation accuracy and numerical efficiency. IBM [21] exhibits similar performance in both accuracy and numerical efficiency, but it requires the model order to be known *a priori*.

Our MOE approach produces accurate results for both low and high SNR. For low SNR, it uses a newly introduced metrics calculated in the frequency domain. The metrics, however, cannot be used at high SNR since it is affected by residuals of the extracted components, similarly to noise variance estimation [13, 15–17]. To address the MOE accuracy at high SNR, we introduce an additional spectrum amplitude threshold which does not include noise variance estimation. In terms of the numerical efficiency, the proposed method outperforms information criterion-based methods [13, 15–17] since it is not based on minimization of a penalized-likelihood function calculated for a set of candidate model orders, with maximal order set high enough to include the correct model order.

The paper is organized as follows. In Section 2, the signal model is given and estimation problem formulated. The proposed method for MOE and frequency estimation of multiple 2-D complex sinusoids is described in Section 3, whereas its performance is evaluated in Section 4. Conclusions are drawn in Section 5. The derivation of probability of false alarm used in sinusoid detection test is given in Appendix A, whereas Appendix B provides the rationale and guidelines for selecting an optimal amplitude threshold value used in detection test at high SNR.

2. Signal model and problem formulation

A 2-D signal under consideration $s(m,n)$ contains K complex sinusoids as follows:

$$s(m,n) = \sum_{k=1}^{K} A_k e^{j(2\pi f_{1k} m + 2\pi f_{2k} n)}, \tag{1}$$

where K represents the number of distinct 2-D frequencies $\{(f_{1k}, f_{2k}), k = 1, 2, \cdots, K\}$, A_k is complex amplitude of the k-th component, and $0 \leq m \leq M-1$ and $0 \leq n \leq N-1$. Phases of complex amplitudes are random real numbers uniformly distributed within $[-\pi, \pi)$. Frequencies satisfy $f_{1k} \in [-0.5, 0.5)$ and $f_{2k} \in [-0.5, 0.5)$. The received signal can be written as

$$x(m,n) = s(m,n) + \xi(m,n), \tag{2}$$

where $\xi(m,n)$ represents 2-D AWGN sequence with zero mean and unknown variance σ_ξ^2, and with i.i.d. real and imaginary parts. We will assume that the number of components K is not *a priori* known. Finally, we allow 2-D sinusoids to have a single matching frequency, i.e., that $f_{1k} = f_{1l}$ or $f_{2k} = f_{2l}$ for $k \neq l$.

In matrix form, relation (2) reads

$$\mathbf{X} = \mathbf{S} + \mathbf{\Xi}, \tag{3}$$

where the $M \times N$ signal matrix $\mathbf{S}$ can be written as

$$\mathbf{S} = \sum_{k=1}^{K} A_k \mathbf{S}_k(f_{1k}, f_{2k}) = \sum_{k=1}^{K} A_k \mathbf{s}_m(f_{1k}) \mathbf{s}_n^\top(f_{2k}), \tag{4}$$

with

$$\begin{aligned} \mathbf{s}_m(f_{1k}) &= [1 \; e^{j2\pi f_{1k}} \; e^{j2\pi 2 f_{1k}} \cdots \; e^{j2\pi(M-1)f_{1k}}]^\top \\ \mathbf{s}_n(f_{2k}) &= [1 \; e^{j2\pi f_{2k}} \; e^{j2\pi 2 f_{2k}} \cdots \; e^{j2\pi(N-1)f_{2k}}]^\top \end{aligned} \tag{5}$$

and $[\cdot]^\top$ representing the transpose operator.

Note that the signal matrix corresponding to the k-th component,

$$\mathbf{S}_k(f_{1k}, f_{2k}) = \mathbf{s}_m(f_{1k}) \mathbf{s}_n^\top(f_{2k}), \tag{6}$$

satisfies the separability condition [7, 8], which enables separate estimation of frequency components f_{1k} and f_{2k}. The matrix $\mathbf{S}_k(f_{1k}, f_{2k})$ is closely related to array manifold $\mathbf{a}(\theta, \phi)$ of planar arrays, which also satisfies the separability condition.

This paper addresses estimation of the number of 2-D complex sinusoids K and their frequencies $\{(f_{1k}, f_{2k}), k = 1, 2, \cdots, K\}$ from the matrix $\mathbf{X}$. Once these frequencies are estimated, complex amplitudes A_k, $k = 1, 2, \cdots, K$ can be estimated via iterative approach presented in [21].

3. Proposed 2-D frequency estimation

Due to its discrete nature, 2-D DFT maximization generally yields frequency estimations displaced from the true frequencies and a refinement is required to improve the estimation accuracy. In this paper, we propose a two-stage procedure for frequency estimation. In both stages, owing to the separability condition (6), 2-D frequency estimation is carried out via two 1-D estimations, one along each frequency dimension,

which leads to significant computational savings. For 1-D frequency estimation, we use recently proposed three-point 1-D periodogram maximization [22, 23], presented in Section 3.1. In the first stage (Section 3.2), the strongest component is detected by locating maximum of the 2-D DFT, its frequencies are refined and used for removing this component from the spectrum. This procedure is repeated until the remaining spectrum does not contain peaks that can be associated with 2-D complex sinusoids. The first frequency estimation stage, therefore, provides the number of signal components. Since sinusoids affect each other regarding frequency estimation [24], we propose to mitigate the influence of other sinusoids on the one currently processed by removing them from the spectrum of the received signal in the second stage. The second stage (Section 3.3) is crucial in achieving the CRLB of frequency estimation. It uses MOE and frequency estimations provided by the first stage.

3.1. Three-point 2-D periodogram maximization

In this section, the 1-D periodogram maximization procedure [22] is extended to the 2-D periodogram, which is used in both stages of the proposed fine frequency estimation.

The ML frequency estimation of a single 2-D complex sinusoid is obtained as [25]

$$\hat{f}_{\mathrm{ML}} = \arg\max_{\theta_1,\theta_2} P(\theta_1,\theta_2), \tag{7}$$

where the 2-D periodogram $P(\theta_1,\theta_2)$ is defined as

$$P(\theta_1,\theta_2) = \left| \sum_{m=0}^{M-1} \sum_{n=0}^{N-1} x(m,n) e^{-j(2\pi\theta_1 m + 2\pi\theta_2 n)} \right|. \tag{8}$$

θ_1 and θ_2 represent continuous frequencies. The periodogram $P(\theta_1,\theta_2)$ is efficiently calculated using the 2-D DFT. We propose to refine coarse 2-D periodogram maxima using the approach [22] developed for mono-component 1-D sinusoids, based on the Candan's estimation [26] and three-point 2-D periodogram maximization. The method is presented in Table 1.

3.2. Model order estimation and frequency refinement - Stage I

The first refinement stage can be described by the algorithm presented in Table 2. The outputs of this stage are MOE $\hat{K}$ and frequency estimations (f_{1k}^r, f_{2k}^r), $k = 1, 2, \cdots, \hat{K}$.

The sinusoid removal step plays the crucial role in both MOE and frequency estimation. If (f_{1k}^r, f_{2k}^r) is very close to true frequency (f_{1k}, f_{2k}), term $\mathbf{s}_m^*(f_{1k}^r)\,\mathbf{s}_n^{\mathrm{H}}(f_{2k}^r)$ in (12) approximately equals the conjugated version of the signal matrix $\mathbf{S}_k(f_{1k}, f_{2k})$ of the k-th component (see (6)). Then, the element-wise product in (12) will result in demodulation of that component, i.e., its shifting in the 2-D frequency domain towards low-frequency band of $\mathbf{X}^d$. Ideally, if $(f_{1k}^r, f_{2k}^r) = (f_{1k}, f_{2k})$, the demodulated component will occupy only the DC term of $\mathbf{X}^d$. Step 2 removes the demodulated component, whereas step 3 cancels the demodulation effect of step 1. Removing current strongest component from the analysed signal can be performed very

Table 1: Three-point 2-D periodogram maximization

Coarse estimation Calculate the 2-D DFT of matrix $\mathbf{X}$, denoted as $\mathbf{X}_{\mathrm{FT}}(k_1, k_2)$, where k_1 and k_2 represent discrete frequency indices. Locate the maximum position in both dimensions, i.e., find indices k_{10} and k_{20} that maximize $|\mathbf{X}_{\mathrm{FT}}(k_1, k_2)|$.

Candan's estimation Calculate the Candan's displacement [26] in both frequency dimensions:

$$\begin{aligned}\delta_{1C} &= \frac{\arctan\left(\tan(\frac{\pi}{M})\mathrm{Re}\left\{\frac{X_{\mathrm{FT}}(k_{10}-1,k_{20})-X_{\mathrm{FT}}(k_{10}+1,k_{20})}{2X_{\mathrm{FT}}(k_{10},k_{20})-X_{\mathrm{FT}}(k_{10}-1,k_{20})-X_{\mathrm{FT}}(k_{10}+1,k_{20})}\right\}\right)}{\frac{\pi}{M}} \\ \delta_{2C} &= \frac{\arctan\left(\tan(\frac{\pi}{N})\mathrm{Re}\left\{\frac{X_{\mathrm{FT}}(k_{10},k_{20}-1)-X_{\mathrm{FT}}(k_{10},k_{20}+1)}{2X_{\mathrm{FT}}(k_{10},k_{20})-X_{\mathrm{FT}}(k_{10},k_{20}-1)-X_{\mathrm{FT}}(k_{10},k_{20}+1)}\right\}\right)}{\frac{\pi}{N}},\end{aligned} \tag{9}$$

and then the Candan's frequency estimations

$$\begin{aligned} f_{1C} &= \frac{k_{10}+\delta_{1C}}{M} \\ f_{2C} &= \frac{k_{20}+\delta_{2C}}{N}. \end{aligned} \tag{10}$$

In (9) and (10), subscript C stands for *Candan*.

Parabolic interpolation For each frequency dimension $d = 1, 2$, calculate three periodogram samples P_{d1}, P_{d2} and P_{d3} at frequencies $\theta_{d1} = f_{dC} - \Delta_d$, $\theta_{d2} = f_{dC}$ and $\theta_{d3} = f_{dC} + \Delta_d$. Middle frequencies f_{dC} are given by (10). Side frequencies θ_{d1} and θ_{d3} are displaced by Δ_d from f_{dC}. According to [22], Δ_d is chosen to satisfy $\Delta_1 \in (0, \frac{1}{2M}]$ and $\Delta_2 \in (0, \frac{1}{2N}]$, without significantly affecting the final estimation accuracy. The final frequency estimation along the d-th dimension is obtained by calculating the vertex of a parabola fitted through points (θ_{d1}, P_{d1}), (θ_{d2}, P_{d2}) and (θ_{d3}, P_{d3}) [22]

$$\theta_d^{fin} = \frac{1}{2}\frac{\theta_{d3}^2(P_{d1}-P_{d2}) + \theta_{d2}^2(P_{d3}-P_{d1}) + \theta_{d1}^2(P_{d2}-P_{d3})}{\theta_{d3}(P_{d1}-P_{d2}) + \theta_{d2}(P_{d3}-P_{d1}) + \theta_{d1}(P_{d2}-P_{d3})}, \tag{11}$$

where $d = 1, 2$.

efficiently, without calculating the 2-D DFT, following the rationale used in the 1-D case [27]. Namely, since the DC term of $\mathbf{X}^d$ equals the sum of its values, the matrix $\mathbf{X}^\dagger$ defined in (13) can be written as

$$\begin{aligned} \mathbf{X}^\dagger &= \left(\mathbf{X}^d - \overline{\mathbf{X}^d}\right) \circ \left(\mathbf{s}_m(f_{1k}^r)\,\mathbf{s}_n^\top(f_{2k}^r)\right) \\ &= \mathbf{X}^{(k)} - \overline{\mathbf{X}^d}\,\mathbf{s}_m(f_{1k}^r)\,\mathbf{s}_n^\top(f_{2k}^r), \end{aligned} \tag{14}$$

where $\overline{\mathbf{X}^d}$ represents the mean value of $\mathbf{X}^d$, and $\mathbf{X}^d - \overline{\mathbf{X}^d}$ within brackets corresponds to step 2 of the algorithm. Note that, since $\mathbf{s}_m(f_{1k}^r)\,\mathbf{s}_n^\top(f_{2k}^r)$ represents an approximation of the signal matrix $\mathbf{S}_k(f_{1k}, f_{2k})$, relation (14) implies that the k-th component is removed from $\mathbf{X}^{(k)}$ via subtraction as well as that $\overline{\mathbf{X}^d}$ represents an estimation of the complex amplitude A_k.

Table 2: Model order estimation and first frequency refinement

Initialization Set $k = 1$, $\hat{K} = 0$, $\mathbf{X}^{(1)} = \mathbf{X}$ and $M_{X_{\mathrm{FT}}} = P(\theta_1^{fin}, \theta_2^{fin})$, where $(\theta_1^{fin}, \theta_2^{fin})$ represents a fine frequency estimation of the strongest component (see Table 1).

Loop

Sinusoid detection If the spectrum of $\mathbf{X}^{(k)}$ does not contain peaks that can be associated with sinusoids, output MOE $\hat{K}$ and frequency estimations (f_{1k}^r, f_{2k}^r), $k = 1, 2, \cdots, \hat{K}$, and exit.

Coarse estimation Detect the strongest component by locating maximum of $|\mathbf{X}_{\mathrm{FT}}^{(k)}(k_1, k_2)|$.

Fine estimation Refine coarse frequency estimation using the approach proposed in Section 3.1, resulting in (f_{1k}^r, f_{2k}^r) (r stands for *refined*).

Sinusoid removal Remove the strongest component from $\mathbf{X}^{(k)}$ in the following three steps.

1. Demodulate $\mathbf{X}^{(k)}$ using estimation (f_{1k}^r, f_{2k}^r) as

$$\mathbf{X}^d = \mathbf{X}^{(k)} \circ (\mathbf{s}_m^*(f_{1k}^r)\, \mathbf{s}_n^{\mathrm{H}}(f_{2k}^r)), \tag{12}$$

   where $\mathbf{s}_m(\cdot)$ and $\mathbf{s}_n(\cdot)$ are defined in (5), $[\cdot]^*$ and $[\cdot]^{\mathrm{H}}$ represent the conjugate and Hermitian transpose operators, respectively, whereas $\circ$ represents the element-wise (Hadamard) product.

2. Remove the direct current (DC) term of $\mathbf{X}^d$ which results in a matrix $\mathbf{X}'$.

3. Modulate $\mathbf{X}'$ to obtain the signal matrix $\mathbf{X}^\dagger$ without the strongest component, that is

$$\mathbf{X}^\dagger = \mathbf{X}' \circ (\mathbf{s}_m(f_{1k}^r)\, \mathbf{s}_n^{\top}(f_{2k}^r)). \tag{13}$$

   Set $\hat{K} = k$, $k = k + 1$ and $\mathbf{X}^{(k)} = \mathbf{X}^\dagger$.

End loop

Frequency estimation (f_{1k}^r, f_{2k}^r) obtained in this stage does not meet the CRLB for each component, as will be shown in Section 4. To accomplish this goal, we perform the second refinement stage, as described in Section 3.3.

MOE is carried out within this stage. Step *Sinusoid detection* in Table 2 embodies a sinusoid detection criterion, which will be elaborated in the following subsection. Related to the sinusoid detection is the spectrum maximum $M_{X_{\mathrm{FT}}}$ set in the initialization step in Table 2.

3.2.1. Sinusoid detection

The proposed criterion for sinusoid detection combines two metrics to provide an accurate MOE for a wide SNR range. The first one is calculated as follows:

$$d = \frac{|\mathbf{X}_{\mathrm{FT}}(k_{10}, k_{20})|^2}{\frac{1}{M+N-2}\left(\sum\limits_{\substack{k_1=0 \\ k_1 \neq k_{10}}}^{M-1} |\mathbf{X}_{\mathrm{FT}}(k_1, k_{20})|^2 + \sum\limits_{\substack{k_2=0 \\ k_2 \neq k_{20}}}^{N-1} |\mathbf{X}_{\mathrm{FT}}(k_{10}, k_2)|^2\right)}, \tag{15}$$

where k_{10} and k_{20} maximize $|\mathbf{X}_{\mathrm{FT}}(k_1, k_2)|^2$ along k_1 and k_2, respectively, i.e.

$$|\mathbf{X}_{\mathrm{FT}}(k_{10}, k_{20})| = \max_{k_1, k_2} |\mathbf{X}_{\mathrm{FT}}(k_1, k_2)|^2.$$

In the absence of sinusoids, both the numerator and denominator of d represent estimates of noise variance, using 1 and $M+N-2$ samples, respectively. In addition, they are independent of each other since all random variables forming them are distinct, i.e., $|\mathbf{X}_{\mathrm{FT}}(k_{10}, k_{20})|^2$ does not appear in the denominator. Finally, statistics of d does not depend on the noise variance σ_ξ^2 since the numerator and summation terms within the denominator are linearly dependent on σ_ξ^2 which therefore cancels out in quotient d.

The sinusoid detection problem reduces to the following binary hypothesis test:

$$d \underset{\mathcal{H}_0}{\overset{\mathcal{H}_1}{\gtrless}} \gamma_L, \tag{16}$$

where the null hypothesis $\mathcal{H}_0$ and the alternative hypothesis $\mathcal{H}_1$ are given as

$$\begin{aligned} &\mathcal{H}_0 : \text{Sinusoid is absent } (\mathbf{X} = \mathbf{\Xi}) \\ &\mathcal{H}_1 : \text{Sinusoid is present } (\mathbf{X} = \mathbf{S} + \mathbf{\Xi}), \end{aligned} \tag{17}$$

and γ_L represents the detection threshold. The value of γ_L will be selected so that the probability of false alarm (PFA)

$$P_{\mathrm{FA}} = P(d \geq \gamma_L; \mathcal{H}_0) \tag{18}$$

is fixed. For the metric d given by (15), the PFA equals

$$P_{\mathrm{FA}} = \left(\frac{\gamma_L}{M+N-2} + 1\right)^{-(M+N-2)}. \tag{19}$$

Derivation details are given in Appendix A. From (19), the threshold γ_L is obtained as

$$\gamma_L = (M+N-2)\left(P_{\mathrm{FA}}^{-\frac{1}{M+N-2}} - 1\right). \tag{20}$$

For high SNR, residuals of the removed sinusoids become significant compared with noise, and test (16) may lead to overestimating the number of sinusoids. To take residuals into account, we introduce an amplitude threshold as a percentage ϵ of the spectrum maximum prior to removing any component ($M_{X_{\mathrm{FT}}}$

in Table 2). Selection of ϵ is driven by two contradictory requirements. The first one dictates ϵ to be as big as possible in order to prevent residuals from being counted as separate components. The other one dictates ϵ to be as small as possible to enable detection of sinusoids of a wide amplitude range. Therefore, ϵ should quantify a boundary between the weakest component and residual of the strongest one. Selecting a proper ϵ value is affected by several factors, including the SNR, total number of components and their relative position in the 2-D frequency plane, which make an analytical optimization practically infeasible. Appendix B provides rationale and guidelines for selecting an optimal ϵ value, ϵ_{opt}, given by (31), which is numerically justified in Example 3 in Section 4.

The proposed criterion for sinusoid detection states that the spectrum of $\mathbf{X}$ contains peaks that can be associated with 2-D complex sinusoids if the following two conditions are met:

$$\begin{gathered} d \geq \gamma_L \\ \text{and} \\ |\mathbf{X}_{\text{FT}}(k_{10}, k_{20})| > \epsilon_{\text{opt}} M_{X_{\text{FT}}}, \end{gathered} \tag{21}$$

where $|\mathbf{X}_{\text{FT}}(k_{10}, k_{20})|$ represents the current spectrum maximum. For low SNR (hence L in γ_L), MOE is affected by the first condition, whereas the second one prevents overestimation at high SNR. Criterion (21) is checked in the *Sinusoid detection* step in Table 2.

The proposed sinusoid detection has been motivated by approaches for detection of well-focused objects in SAR/ISAR images [28, 29]. In addition to complex sinusoids, models in [28, 29] included polynomial-phase signals [28] and sinusoidal frequency modulated signals [29].

Finally, note that the proposed MOE can be used with any iterative 2-D frequency estimation method based on sinusoid detection, parameter estimation and cancellation, e.g., in [21].

3.3. Frequency refinement - Stage II

In order to reduce the influence of sinusoids on each other during the frequency estimation, we propose to remove all sinusoids from the received signal matrix except for the one to be estimated [27, 30]. After that, 2-D periodogram maximization, as an ML approach for single frequency estimation, is used.

The outputs of Stage I are MOE $\hat{K}$ and frequency estimations (f_{1k}^r, f_{2k}^r), $k = 1, 2, \cdots, \hat{K}$. Improving the estimation accuracy with respect to Stage I is carried out following the algorithm presented in Table 3.

Removing all 2-D sinusoids from $\mathbf{X}$ except for the one currently processed is carried out iteratively by repeating the *Sinusoid removal* step in Table 2 $\hat{K} - 1$ times with (f_{1l}^r, f_{2l}^r) in place of (f_{1k}^r, f_{2k}^r) in (12) and (13), $l = 1, 2, \cdots, \hat{K}$ and $l \neq k$. Relation (14) enables removal without calculating the 2-D DFT.

Note that the proposed sinusoid removal approach is analogous to that used in [21] (originally proposed in [20] for 1-D case). In [21], frequencies and amplitude of the current sinusoid have been estimated after the leakage terms of the other ones have been iteratively removed. In our case, we also cancel all other sinusoids

Table 3: Second frequency refinement

For $k = 1, 2, \cdots, \hat{K}$

Removal of other sinusoids Remove all 2-D sinusoids from the received signal matrix $\mathbf{X}$, except the k-th one, using estimations (f_{1l}^r, f_{2l}^r), $l = 1, 2, \cdots, \hat{K}$, $l \neq k$, in step *Sinusoid removal* in Table 2.

Final frequency estimation For frequency dimensions $d = 1, 2$, calculate three periodogram samples P_{d1}, P_{d2} and P_{d3} at frequencies $\theta_{d1} = f_{dk}^r - \Delta_d$, $\theta_{d2} = f_{dk}^r$ and $\theta_{d3} = f_{dk}^r + \Delta_d$. Calculate the final frequency estimations θ_d^{fin}, $d = 1, 2$, according to (11) in Table 1 and update frequency estimations as $f_{dk}^r = \theta_d^{fin}$, $d = 1, 2$.

End for

(step *Removal of other sinusoids* in Table 3) prior to the final frequency estimation of the current one. In that sense, term $\overline{\mathbf{X}^d}$ in (14) represents an estimation of the complex amplitude of the current sinusoid after all other sinusoids have been cancelled out.

4. Numerical results

In this section, performance of the proposed model is evaluated through the MSE of frequency estimation and percentage of correct order estimation (PCOE). To determine an optimal ϵ to be used in the proposed MOE (see (21)), we introduce percentage of high PCOE (PH-PCOE) as follows:

$$\text{PH-PCOE}_{\gamma_L}(\epsilon) = \frac{\sum_{i=1}^{N_{\text{SNR}}} [\![\text{PCOE}_{\epsilon,\gamma_L}(\text{SNR}(i)) \geq T_{\text{PCOE}}]\!]}{N_{\text{SNR}}}, \tag{22}$$

where $\text{PCOE}_{\epsilon,\gamma_L}(\text{SNR}(i))$ represents the value of PCOE calculated for given $\text{SNR}(i)$ and with parameters ϵ and γ_L, N_{SNR} represents the number of considered SNR values, T_{PCOE} is high threshold in the PH-PCOE calculation and $[\![\cdot]\!]$ is the Iverson bracket defined as

$$[\![S]\!] = \begin{cases} 1, & \text{statement } S \text{ is true} \\ 0, & \text{otherwise.} \end{cases}$$

The parameter γ_L will be calculated according to the predefined PFA (relation (20)). On the other hand, the optimal ϵ will be obtained via

$$\epsilon_{\text{opt}} = \underset{\epsilon}{\text{argmax}}\ \text{PH-PCOE}_{\gamma_L}(\epsilon). \tag{23}$$

The SNR of the k-th sinusoid component is calculated as

$$\text{SNR}_k = 10 \log_{10} \frac{|A_k|^2}{\sigma_\xi^2}. \tag{24}$$

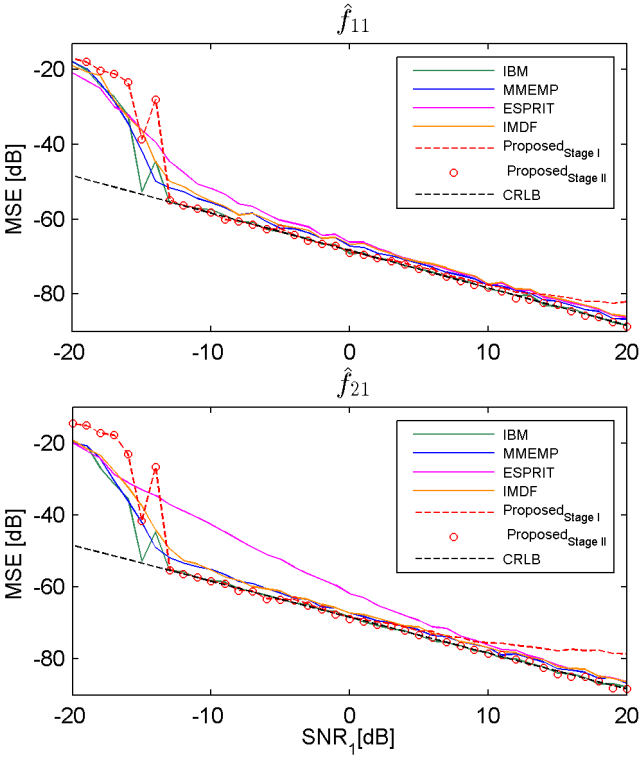

Figure 1: MSE of three-component 2-D complex sinusoid frequency estimation (strongest component) - Case of different frequencies along each dimension.

In this section, the MSE, PCOE and PH-PCOE values are averaged over 300 Monte-Carlo simulations.

Example 1: We first consider $K = 3$ sinusoids with frequencies $(f_{11}, f_{21}) = (0.103, 0.319)$, $(f_{12}, f_{22}) = (0.329, 0.189)$, $(f_{13}, f_{23}) = (0.204, 0.418)$, and amplitudes $|A_1| = 1$, $|A_2| = 0.9$ and $|A_3| = 0.8$. The signal size is $M \times N = 32 \times 32$. The MSE performances of the proposed method, IBM [21], MMEMP [3], ESPRIT [11] and IMDF [2] are presented in Figs. 1 and 2 for the strongest and weakest components, respectively. For the proposed method, the MSEs of both Stage I and Stage II are depicted. From Fig. 1, we conclude that Stage I is not sufficient to attain the CRLB for higher SNR values, which is due to the fact that frequency estimation of the strongest component is influenced by the presence of weaker ones. In Stage II, however, this influence is attenuated by removing weaker sinusoids from the considered signal prior to final frequency estimation. On the other hand, both stages perform similarly for the weakest component, as presented in Fig. 2. Stage II brings no significant accuracy improvement for this component since it is estimated in Stage I after all other components have already been removed. The IBM, MMEMP and IMDF estimators perform very well, whereas the ESPRIT-based estimation is outperformed by other techniques, especially for lower SNR. Nonetheless, ESPRIT approaches the CRLB for higher SNR.

Example 2: Sinusoids with a single matching frequency are considered. The signal contains five sinu-

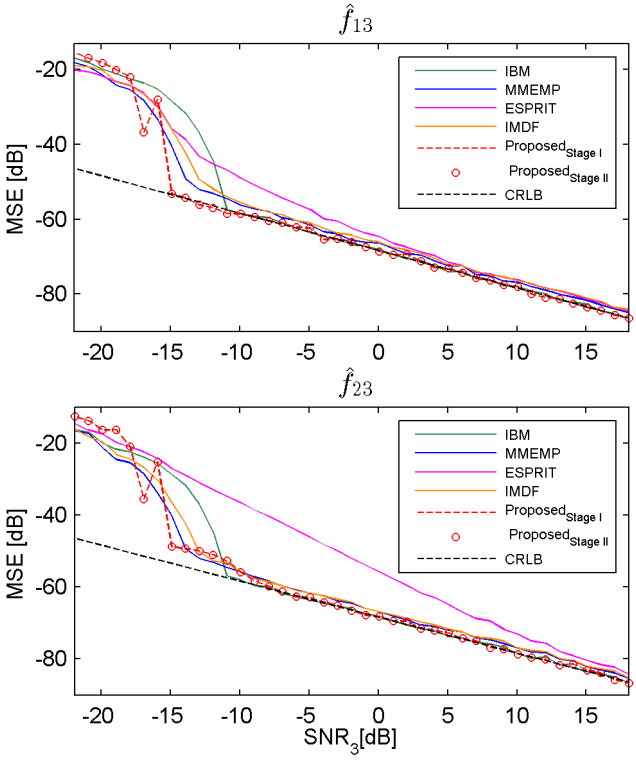

Figure 2: MSE of three-component 2-D complex sinusoid frequency estimation (weakest component) - Case of different frequencies along each dimension.

soids with parameters $(f_{11}, f_{21}) = (0.107, 0.308)$, $(f_{12}, f_{22}) = (0.308, -0.189)$, $(f_{13}, f_{23}) = (0.107, -0.189)$, $(f_{14}, f_{24}) = (0.403, -0.227)$, $(f_{15}, f_{25}) = (-0.371, -0.039)$, $|A_1| = 1$, $|A_2| = 0.95$, $|A_3| = 0.9$, $|A_4| = 0.8$ and $|A_5| = 0.75$. The MSE curves for the strongest and the weakest component are presented in Figs. 3 and 4, respectively. IMDF was left out in this example since it cannot resolve components with equal frequencies [2]. IBM and the proposed method (Stage II) reach the CLRB, whereas MMEMP and ESPRIT are characterized by a small bias. Again, in the proposed method, Stage I does not suffice to reach the CRLB, which can be seen from the bottom plot of Fig. 3. This is not the case for the weakest component (Fig. 4), whose estimation accuracy meets the CRLB for both Stage I and II.

Overall, the proposed method outperforms MMEMP, ESPRIT and IMDF in terms of the estimation accuracy and calculation complexity. On the other hand, its performance is on par with that of IBM in terms of both accuracy and complexity. However, as opposed to all other considered methods, the proposed one does not require the number of components to be known in advance.

Example 3: Let us now determine the optimal value for parameter ϵ used in criterion (21). To that end, we calculate PH-PCOE defined in (22) with $T_{\text{PCOE}} = 0.99$ and $P_{\text{FA}} = 5 \times 10^{-6}$. The signal from Example 2 is considered. Figure 5 presents PH-PCOE$_{\gamma_L}(\epsilon)$ obtained for $\epsilon \in [0, 1]$ with a step of 0.05. The optimal ϵ

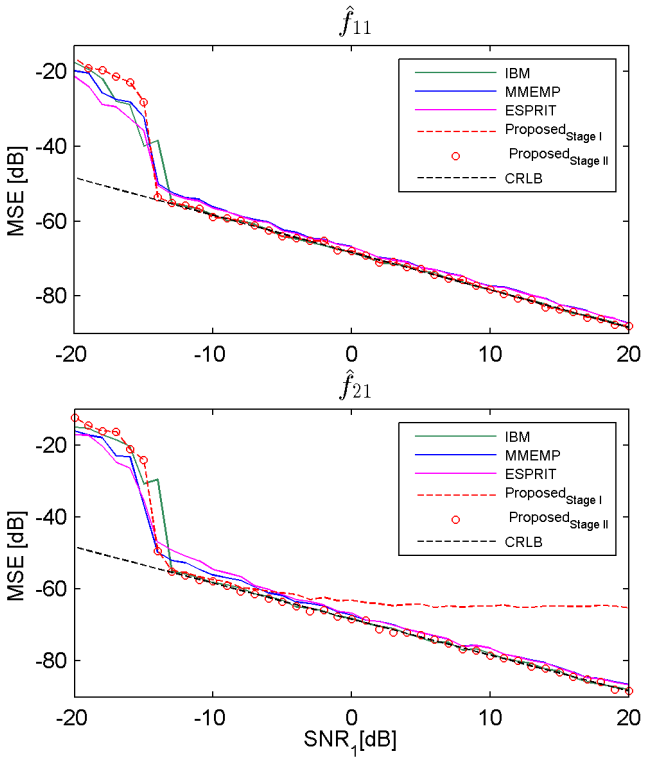

Figure 3: MSE of five-component 2-D complex sinusoid frequency estimation (strongest component) - Case of equal frequencies along one dimension.

according to (23) is $\epsilon_{\text{opt}} = 0.065$. Note that PH-PCOE$_{\gamma_L}(\epsilon)$ is practically flat and maximal for a wide range of ϵ values. For the optimal ϵ value, we will select a point where this flat region starts in order to allow as big amplitude difference between the components as possible, as discussed in Section 3.2.1. Note also that the numerically obtained ϵ_{opt} has a clear analytical justification presented in Appendix B.

Example 4: Here we compare the proposed MOE method with BIC, AIC and EEF, generalized for 2-D complex exponential signals in [13] on the signal from Example 2. In BIC/AIC/EEF, maximal model order used in calculating and minimizing penalized-likelihood function was set to 7. In the proposed method, we use $P_{\text{FA}} = 5 \times 10^{-6}$ and $\epsilon_{\text{opt}} = 0.065$ obtained in Example 3. The PCOE curves are presented in Fig. 6, showing that the proposed method does not suffer from overestimation at high SNR as opposed to the competing approaches. It is numerically efficient, with the 2-D DFT as its most demanding operation and it does not require estimation of noise variance as the other approaches [13].

5. Conclusions

The paper considers frequency estimation of multiple 2-D complex sinusoids in AWGN. Estimation is performed in the frequency domain, using the DFT as the main tool. Coarse estimates, obtained by locating

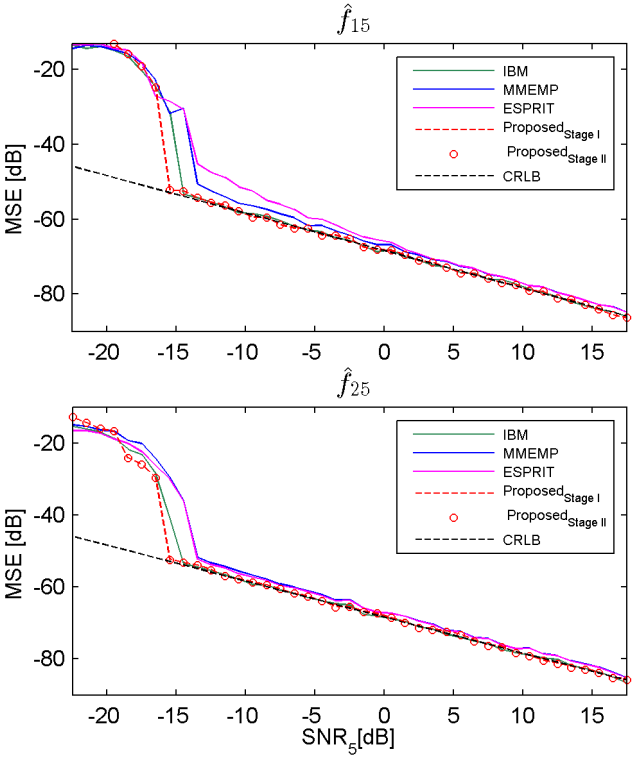

Figure 4: MSE of five-component 2-D complex sinusoid frequency estimation (weakest component) - Case of equal frequencies along one dimension.

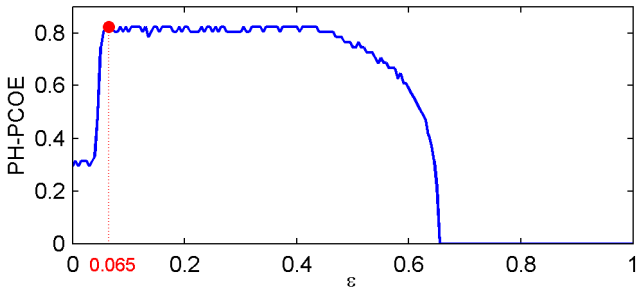

Figure 5: Percentage of high PCOE (PH-PCOE) for setup in Example 2. Optimal ϵ corresponds to the lowest ϵ (0.065 in this example) where PH-PCOE reaches maximum.

maxima in the 2-D DFT of the received signal, are refined in two stages. The first stage provides MOE and frequency estimation improvement with respect to the coarse estimates. The second stage serves to mitigate the influence of sinusoids on each other during frequency estimation, thus improving results of the first stage to the CRLB precision. The proposed frequency estimation outperforms parametric methods in terms of the accuracy and calculation complexity. Compared with the state-of-the-art MOE approaches, the proposed approach provides more accurate results, especially at high SNR, and is characterized by significantly lower

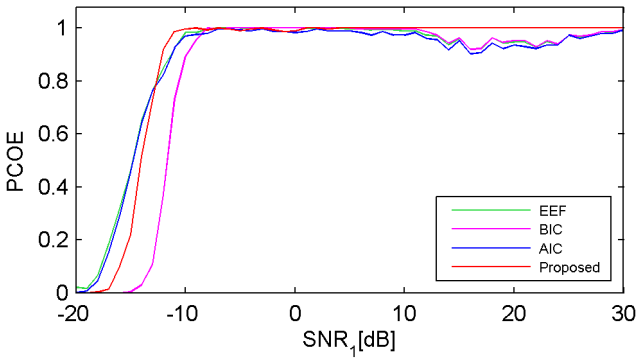

Figure 6: PCOE for the case of five-component signal.

calculation complexity.

Appendix A

In this appendix, we derive the PFA given by (19). To that end, let us analyze the numerator and denominator of d given by (15). Since $\xi(m,n)$ is zero-mean AWGN with variance σ_ξ^2 and i.i.d. real and imaginary parts, the 2D DFT of $\xi(m,n)$ is also complex AWGN with zero mean and variance $MN\sigma_\xi^2$. Since the variance term exists in both the numerator and denominator of d, we can cancel it out, i.e., we can view the terms in the numerator and denominator of d as standard normal variables (zero mean and unit variance). In that case, the numerator and denominator of d are independent chi-square variables with 2 and $2(M+N-2)$ degrees of freedom, respectively [31]. The ratio of two independent chi-square variables, Y_1 and Y_2, divided by the corresponding degrees of freedom k_1 and k_2, i.e.

$$Z = \frac{Y_1/k_1}{Y_2/k_2},$$

is a random variable which conforms to the F-distribution with parameters k_1 and k_2, i.e., $Z \sim F(k_1,k_2)$ [31]. Therefore, the metric d has an F-distribution with parameters 2 and $2(M+N-2)$, i.e., $d \sim F(2,2(M+N-2))$. The PFA (18) hence equals

$$\begin{aligned} P_{\text{FA}} &= P(d \geq \gamma_L; \mathcal{H}_0) \\ &= 1 - F_d(\gamma_L; 2, 2(M+N-2)) \\ &= 1 - I_{\frac{2\gamma_L}{2\gamma_L+2(M+N-2)}}(1, M+N-2), \end{aligned} \tag{25}$$

where $F_Z(z;k_1,k_2)$ is the cumulative distribution function (CDF) of an F-distributed variable Z with parameters k_1 and k_2, and $I_x(a,b)$ is the regularized incomplete beta function [31]. Since it holds

$$I_x(1,b) = 1-(1-x)^b,$$

the PFA reduces to

$$\begin{aligned} P_{\mathrm{FA}} &= \left(1 - \frac{\gamma_L}{\gamma_L + M + N - 2}\right)^{M+N-2} \\ &= \left(\frac{M+N-2}{\gamma_L + M + N - 2}\right)^{M+N-2} \\ &= \left(\frac{\gamma_L}{M+N-2} + 1\right)^{-(M+N-2)}, \end{aligned} \tag{26}$$

which concludes the PFA derivation.

Appendix B

The frequency estimation accuracy plays the crucial role in selecting a proper value of ϵ. The lower the accuracy the stronger the residual after component removal and hence the higher ϵ_{opt} should be adopted. In addition to the signal size and the SNR, the estimation accuracy of the strongest component is affected by the total number of components and their relative position in the 2-D frequency plane (vicinity of components and frequency matching). Analytical derivation of an optimal value of ϵ is therefore practically infeasible. However, we will present a rationale for estimating an optimal ϵ, which will be numerically justified in Section 4.

Figure 7 depicts the main lobe of the 2-D periodogram of a demodulated noise-free 2-D complex sinusoid. When the estimated and true frequencies coincide, only the central 2-D DFT sample is not zero (squares in Fig. 7). However, when the estimated and true frequencies differ, all 2-D DFT samples have non-zero values (circles in Fig. 7). In that case, the 2-D DFT maximum (sample P_0) is shifted from the true 2-D periodogram maximum by δ_1 and δ_2 in θ_1 and θ_2 directions, respectively. The sinusoid removal performance, therefore, depends on the values of displacements δ_1 and δ_2, i.e., the bigger the displacement the more residual remains after the removal. The measure of removal is the value of the second largest 2-D DFT sample (sample P_1 in Fig. 7), i.e., selecting an optimal ϵ should be driven by the ratio of P_1 and P_0.

Statistics of δ_1 and δ_2 are affected by several factors, including the SNR, total number of components and their relative position (higher influence on each other in case of close components), which render precise analytical derivation practically infeasible. However, a guidance regarding selecting a proper value of ϵ in general case can be provided as follows. Since the MSE represents a measure of frequency estimation error, i.e., of displacements δ_1 and δ_2, we can estimate δ_1 and δ_2 as follows:

$$\delta_d = \eta\sqrt{\mathrm{MSE}_d}, \qquad d = 1, 2, \tag{27}$$

where MSE_d represents the MSE of frequency estimation f_{dk}, $d = 1, 2$, whereas η represents a scaling coefficient. To estimate MSE_d, we will use the asymptotic CRLBs (ACRLBs) derived in [32, rel. (17)] for

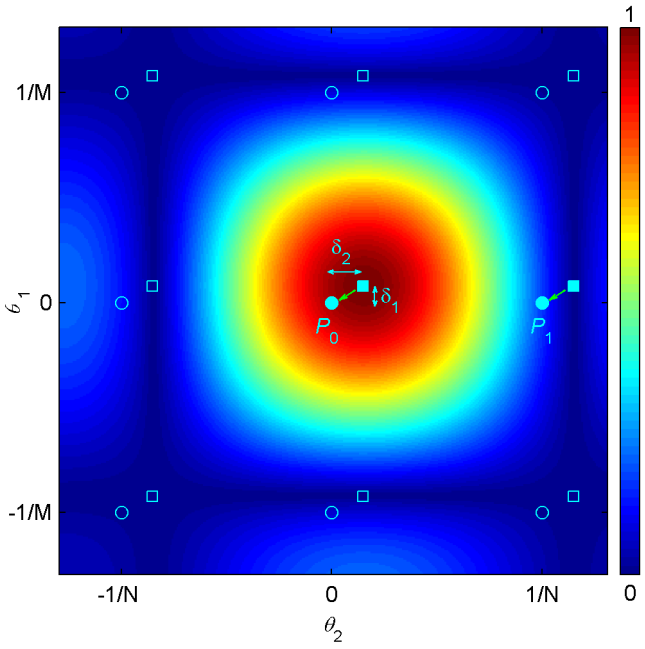

Figure 7: Main lobe of amplitude-normalized 2-D periodogram of a demodulated complex sinusoid (noise-free case) and position of 2-D DFT samples (squares and circles). Squares represent optimal 2-D sampling (estimated and true frequencies coincide), circles realistic 2-D sampling (estimated and true frequencies do not coincide). P_0 represents the 2-D DFT maximum displaced from the true 2-D periodogram maximum by δ_1 and δ_2 in θ_1 and θ_2 directions, respectively. P_1 represents the second strongest 2-D DFT sample.

$M \gg 1$ and $N \gg 1$:

$$\begin{aligned} \mathrm{ACRLB}(f_{1k}) &= \frac{6}{(2\pi)^2 M^3 N \mathrm{SNR}_k}, \\ \mathrm{ACRLB}(f_{2k}) &= \frac{6}{(2\pi)^2 N^3 M \mathrm{SNR}_k}, \end{aligned} \tag{28}$$

where $\mathrm{SNR}_k = \frac{|A_k|^2}{\sigma_\xi^2}$ is the SNR of the k-th component.

Since MOE is carried out in Stage I, frequency estimation (f_1^r, f_2^r) of the strongest component does not meet the CRLB which is reflected in MSE saturation (for a specific case, see Fig. 3 (bottom) where the saturation occurs at around -6 dB). Hence, for the MSE in (27), we should use the ACRLB calculated for SNR where the MSE saturation begins, denoted as SNR_{sat}.

Following the three-sigma rule [33], the value of η in (27) should be set above 3, say $\eta = 3.5$.

When noise is present, the values of P_0 and P_1 also depend on the noise variance. Since $\xi(m,n)$ is zero-mean AWGN with variance σ_ξ^2 and i.i.d. real and imaginary parts, the 2-D DFT of $\xi(m,n)$, $\boldsymbol{\Xi}_{\mathrm{FT}}$, is also complex AWGN with zero mean and variance $MN\sigma_\xi^2$ [27]. In that case, $|\boldsymbol{\Xi}_{\mathrm{FT}}|^2$ has a gamma distribution with shape $k = 1$ and scale $\theta = MN\sigma_\xi^2$ [31].

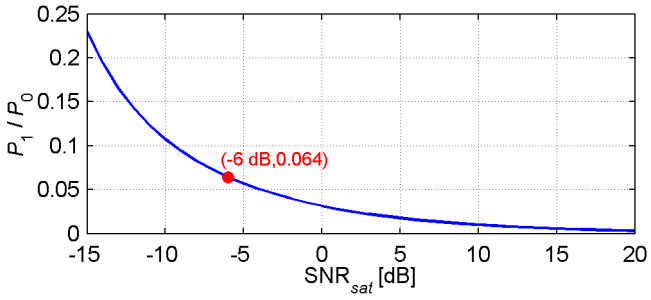

Figure 8: Ratio of the second strongest and the strongest spectrum sample. SNR$_{sat}$ represents the SNR point where the frequency estimation MSE of the strongest component goes into MSE saturation. Red dot corresponds to the MSE saturation point observed in Fig. 3 (bottom).

Taking all previously said into consideration, we will estimate amplitudes P_0 and P_1 as follows:

$$P_0 = \sqrt{\mathrm{E}\left[P^2\left(-\delta_1, -\delta_2\right)\right]} = \sqrt{S^2\left(-\delta_1, -\delta_2\right) + \mathrm{E}\left[|\Xi_{\mathrm{FT}}|^2\right]} = \sqrt{S^2\left(-\delta_1, -\delta_2\right) + MN\sigma_\xi^2},$$
$$P_1 = \sqrt{\mathrm{E}\left[P^2\left(-\delta_1, 1/N - \delta_2\right)\right]} = \sqrt{S^2\left(-\delta_1, 1/N - \delta_2\right) + \mathrm{E}\left[|\Xi_{\mathrm{FT}}|^2\right]} = \sqrt{S^2\left(-\delta_1, 1/N - \delta_2\right) + MN\sigma_\xi^2}, \tag{29}$$

where E[·] represents the expectation operator, $P(\theta_1, \theta_2)$ the 2-D periodogram of the noisy signal (defined in (8)) and $S(\theta_1, \theta_2)$ the 2-D periodogram of a zero-frequency complex sinusoid, i.e., of a 2-D rectangular pulse given as

$$S(\theta_1, \theta_2) = MN|A_k| \left|\frac{\mathrm{sinc}(M\theta_1)}{\mathrm{sinc}(\theta_1)}\right| \left|\frac{\mathrm{sinc}(N\theta_2)}{\mathrm{sinc}(\theta_2)}\right| \tag{30}$$

where sinc(x) represents the normalized sinc function $\mathrm{sinc(x)} = \frac{\sin(\pi x)}{\pi x}$. In (29), the expected value of a gamma distributed variable $|\Xi_{\mathrm{FT}}|^2$ equals the product of shape and scale parameters k and θ [31]. Finally, the optimal ϵ will be calculated as follows:

$$\epsilon_{\mathrm{opt}} = \frac{P_1}{P_0}. \tag{31}$$

The proposed ϵ_{opt} will be verified on a specific case of five components considered in Example 2 in Section 4. Figure 8 depicts the P_1/P_0 ratio calculated versus SNR$_{sat}$. The setup considered in Example 2, with SNR$_{sat}$ $= -6$dB, yields $\epsilon_{\mathrm{opt}} = 0.064$ (red dot in Fig. 8), which is almost identical to the value of 0.065 obtained in Example 3 which deals with numerical optimization of the value of ϵ.

For general case, SNR$_{sat}$ cannot be known in advance. However, since ϵ_{opt} is introduced in criterion (21) to address sinusoid detection at high SNR, there is no need to set SNR$_{sat}$ too low. The binary hypothesis test (16) incorporated in (21) deals with low SNR values.

References

[1] Y. Hua, Estimating two-dimensional frequencies by matrix enhancement and matrix pencil, IEEE Transactions on Signal Processing 40 (9) (1992) 2267–2280.

[2] J. Liu, X. Liu, An eigenvector-based approach for multidimensional frequency estimation with improved identifiability, IEEE Transactions on Signal Processing 54 (12) (2006) 4543–4556.

[3] F.-J. Chen, C. C. Fung, C.-W. Kok, S. Kwong, Estimation of two-dimensional frequencies using modified matrix pencil method, IEEE Transactions on Signal Processing 55 (2) (2007) 718–724.

[4] S. Rouquette, M. Najim, Estimation of frequencies and damping factors by two-dimensional ESPRIT type methods, IEEE Transactions on Signal Processing 49 (1) (2001) 237–245.

[5] F. K. Chan, H.-C. So, W. Sun, Subspace approach for two-dimensional parameter estimation of multiple damped sinusoids, Signal Processing 92 (9) (2012) 2172–2179.

[6] M. A. Richards, Fundamentals of radar signal processing, Tata McGraw-Hill Education, 2005.

[7] H. L. Van Trees, Optimum array processing: Part IV of detection, estimation, and modulation theory, John Wiley & Sons, 2004.

[8] P. Heidenreich, A. M. Zoubir, M. Rubsamen, Joint 2-D DOA estimation and phase calibration for uniform rectangular arrays, IEEE Transactions on Signal Processing 60 (9) (2012) 4683–4693.

[9] C. R. Rao, L. Zhao, B. Zhou, Maximum likelihood estimation of 2-D superimposed exponential signals, IEEE Transactions on Signal Processing 42 (7) (1994) 1795–1802.

[10] M. P. Clark, L. L. Scharf, Two-dimensional modal analysis based on maximum likelihood, IEEE Transactions on Signal Processing 42 (6) (1994) 1443–1452.

[11] M. Haardt, K. Huper, J. B. Moore, J. A. Nossek, Simultaneous schur decomposition of several matrices to achieve automatic pairing in multidimensional harmonic retrieval problems, in: European Signal Processing Conference, 1996. EUSIPCO 1996. 8th, IEEE, 1996, pp. 1–4.

[12] X. Liu, N. D. Sidiropoulos, Almost sure identifiability of constant modulus multidimensional harmonic retrieval, IEEE Transactions on Signal Processing 50 (9) (2002) 2366–2368.

[13] A. Porwal, S. Mitra, A. Mitra, Order estimation of 2-dimensional complex superimposed exponential signal model using exponentially embedded family (EEF) rule: large sample consistency properties, Multidimensional Systems and Signal Processing 30 (3) (2019) 1293–1308.

[14] U. Soverini, T. Söderström, 2D-frequency domain identification of complex sinusoids in the presence of additive noise, IFAC-PapersOnLine 51 (15) (2018) 820–825.

[15] P. Stoica, P. Babu, Model order estimation via penalizing adaptively the likelihood (PAL), Signal Processing 93 (11) (2013) 2865–2871.

[16] P. Stoica, P. Babu, On the exponentially embedded family (EEF) rule for model order selection, IEEE Signal Processing Letters 19 (9) (2012) 551–554.

[17] K. Surana, S. Mitra, A. Mitra, P. Stoica, Estimating the order of sinusoidal models using the adaptively penalized likelihood approach: Large sample consistency properties, Signal Processing 128 (2016) 204–211.

[18] S. Mitra, A. Porwal, Order estimation of superimposed nonlinear complex cisoid model using adaptively penalizing likelihood rule: Consistency results, DEStech Transactions on Engineering and Technology Research (2017).

[19] M. G. Christensen, A. Jakobsson, Multi-pitch estimation, Synthesis Lectures on Speech & Audio Processing 5 (1) (2009) 1–160.

[20] S. Ye, E. Aboutanios, Rapid accurate frequency estimation of multiple resolved exponentials in noise, Signal Processing 132 (2017) 29–39.

[21] J. Wang, W. Sun, L. Huang, J. Zhang, Accurate and computationally efficient interpolation-based method for two-dimensional harmonic retrieval, Digital Signal Processing 78 (2018) 108–120.

[22] S. Djukanović, T. Popović, A. Mitrović, Precise sinusoid frequency estimation based on parabolic interpolation, in: Telecommunications Forum (TELFOR), 2016 24th, IEEE, 2016, pp. 1–4.

[23] S. Djukanović, Sinusoid frequency estimator with parabolic interpolation of periodogram peak, in: Telecommunications and Signal Processing (TSP), 2017 40th International Conference on, IEEE, 2017, pp. 470–473.

[24] D. C. Rife, R. R. Boorstyn, Multiple tone parameter estimation from discrete-time observations, Bell System Technical Journal 55 (9) (1976) 1389–1410.

[25] S. M. Kay, Modern Spectral Estimation: Theory and Application, Prentice Hall; 1 edition, 1999.

[26] Ç. Candan, Analysis and further improvement of fine resolution frequency estimation method from three DFT samples, IEEE Signal Processing Letters 20 (9) (2013) 913–916.

[27] S. Djukanović, V. Popović-Bugarin, Efficient and accurate detection and frequency estimation of multiple sinusoids, IEEE Access 7 (2019) 1118–1125.

[28] V. Popović, I. Djurović, LJ. Stanković, T. Thayaparan, M. Daković, Autofocusing of SAR images based on parameters estimated from the PHAF, Signal Processing 90 (5) (2010) 1382–1391.

[29] LJ. Stanković, T. Thayaparan, M. Daković, V. Popović-Bugarin, Micro-Doppler removal in the radar imaging analysis, IEEE Transactions on Aerospace and Electronic Systems 49 (2) (2013) 1234–1250.

[30] S. Djukanović, An accurate method for frequency estimation of a real sinusoid, IEEE Signal Processing Letters 23 (7) (2016) 915–918.

[31] M. Abramowitz, I. A. Stegun, R. H. Romer, Handbook of mathematical functions with formulas, graphs, and mathematical tables (1988).

[32] R. Boyer, Deterministic asymptotic Cramér–Rao bound for the multidimensional harmonic model, Signal Processing 88 (12) (2008) 2869–2877.

[33] A. Papoulis, U. S. Pillai, Probability, random variables, and stochastic processes, McGraw Hill Higher Education; 4th edition, 2002.